Physica A 462 (2016) 807–815

Contents lists available at ScienceDirect

Physica A

journal homepage: www.elsevier.com/locate/physa

Nonlinear filtering properties of detrended fluctuation analysis

Ken Kiyono *, Yutaka Tsujimoto

Graduate School of Engineering Science, Osaka University, Japan

HIGHLIGHTS

- Systematic investigation on DFA detrending procedure.
- Statistical properties of sliding window DFA are also investigated.
- A quantitative parameter is proposed to quantify local slope instability.

ARTICLE INFO

Article history:
Received 18 February 2016
Received in revised form 13 May 2016
Available online 27 June 2016

Keywords:
Time-series analysis
Fractal
Hurst exponent

ABSTRACT

Detrended fluctuation analysis (DFA) has been widely used for quantifying long-range correlation and fractal scaling behavior. In DFA, to avoid spurious detection of scaling behavior caused by a nonstationary trend embedded in the analyzed time series, a detrending procedure using piecewise least-squares fitting has been applied. However, it has been pointed out that the nonlinear filtering properties involved with detrending may induce instabilities in the scaling exponent estimation. To understand this issue, we investigate the adverse effects of the DFA detrending procedure on the statistical estimation. We show that the detrending procedure using piecewise least-squares fitting results in the nonuniformly weighted estimation of the root-mean-square deviation and that this property could induce an increase in the estimation error. In addition, for comparison purposes, we investigate the performance of a centered detrending moving average analysis with a linear detrending filter and sliding window DFA and show that these methods have better performance than the standard DFA.

1. Introduction

Detrended fluctuation analysis (DFA) has been widely used to assess the presence of long-range correlation and fractal scaling behavior [1–3]. In DFA, to avoid spurious detection of scaling behavior caused by a nonstationary trend embedded in the analyzed time series, a detrending procedure using piecewise least-squares fitting has been applied. An important advantage of DFA over other conventional methods, such as power spectral analysis [4] and rescaled range (R/S) analysis [5], is that it can systematically eliminate nonstationary trends by changing the order of polynomial fitting. In addition, several variants of DFA using different types of detrending techniques have been proposed [6–12]. The performance of DFA and its variants has been tested by a number of numerical studies [3,13–19]. The analytical results of the DFA, such as its asymptotic behavior [20], its relationship with the power spectral density [21], and its relationship with the autocorrelation function [22] have also been reported. However, to lead to better performance of the scaling exponent estimation, criteria

* Corresponding author.
E-mail address: kiyono@bpe.es.osaka-u.ac.jp (K. Kiyono).

http://dx.doi.org/10.1016/j.physa.2016.06.129
0378-4371/

in selecting a method and a guiding principle to improve the DFA methodology have not been clearly established. Empirical evaluations of the estimation performance have demonstrated that the original DFA remains the method of choice in the scaling analysis [16,17,19].

It has been pointed out that the nonlinear filtering properties of the detrending procedure in DFA may induce instabilities in the scaling exponent estimation [10]. However, an explicit link between the nonlinear filtering and the estimation instabilities has not been clearly elucidated. To understand this issue, we here investigate the adverse effects of the DFA detrending procedure on the statistical estimation, and we demonstrate that the nonlinear filtering properties of DFA results in a nonuniformly weighted estimation of the root-mean-square deviation. In addition, it is shown that this property could induce an increase in the estimation error. From the statistical viewpoint, this property is unfavorable and must be improved.

This paper is organized as follows. In Section 2, we briefly review the scaling analysis method used in DFA. In Section 3, we investigate analytically and numerically the nonlinear filtering properties of DFA. In Section 4, we show numerically that the nonlinear detrending filter of DFA induces an increase in the estimation error. Finally, in Section 5, we conclude by discussing a possible improvement of the DFA methodology.

2. Detrended fluctuation analysis

In this section, we briefly review the standard DFA procedure [1–3]. The scaling analysis method using DFA is the following: 1. The analyzed time series $\{x(i)\}$ of length N is integrated after subtracting the mean from each data point:

$$y(k) = \sum_{i=1}^{k} (x(i) - \bar{x}) , \tag{1}$$

where $\bar{x}$ denotes the sample mean of $\{x(i)\}$. 2. The integrated time series $\{y(k)\}_{k=1}^{N}$ is divided into equal-sized, nonoverlapping segments of length n. 3. In each segment, a polynomial function is fitted to $\{y(k)\}$ by the least-squares method, and then the mean-square deviation from the polynomial fit is calculated. 4. The mean-square deviations are averaged over all segments and its square root $F(n)$, referred to as the fluctuation function, is calculated as

$$F(n) = \left[\frac{1}{N_n} \sum_{i=1}^{N_n} \left\{ y(j) - \tilde{y}(j) \right\}^2 \right]^{1/2} , \tag{2}$$

where N_n represents the largest possible length and $\tilde{y}(j)$ is the piecewise least-squares-fitting polynomial. Steps 2 and 3 are repeated over multiple scales (window sizes) to explore the relationship between $F(n)$ and n. The slope of a linear relationship between $\log F(n)$ and $\log n$ provides an estimation of the DFA scaling exponent α.

In DFA, the above step 3 is important to remove the adverse effect caused by any nonstationary trend embedded in the analyzed time series. However, as will be analyzed in the next section, this process acts as a nonlinear high-pass filter. Because of this nonlinearity, well-established linear analysis tools, such as the frequency response based on frequency domain analysis, cannot be employed to investigate the methodological properties of DFA. To overcome this difficulty, we recently proposed a method of analyzing the single-frequency response in the time domain [21]. In this paper, using a similar approach, nonlinear filtering properties of DFA will be investigated.

3. Nonlinear properties of the detrending filter in DFA

In this section, we study in detail properties of the detrending procedure in DFA. In addition, for a comparison purpose, we also consider centered detrending moving average (DMA) analysis [10]. By numerical and analytical studies, it has been demonstrated that the performance of DMA is comparable with that of DFA [19]; in particular, mth-order centered DMA, where m is a nonnegative even integer, is very well comparable with that of $(m + 1)$th-order DFA [23]. These two methods differ only in the detrending procedure. As shown in Fig. 1(a) and (b), the detrending procedure in DFA acts as a nonlinear high-pass filter. Namely, a single-frequency component [Fig. 1(a)] is deformed into a distorted shape [Fig. 1(b)] through this type filter. Moreover, it generates higher frequency components. As shown in Fig. 2, the power spectrum of the filtered output [Fig. 2(b)] indicates higher frequency components. In contrast, in centered DMA in which a moving average,

$$\tilde{y}(i) = \sum_{j=i-(n-1)/2}^{i+(n-1)/2} y(j), \tag{3}$$

is employed instead of the piecewise least-squares fitting, the detrending procedure acts as a linear high-pass filter [Fig. 1(c) and (d)]. As is already well known [10], the detrending moving average filter has no phase shift, and its frequency response (gain) is given by $1 - \sin(\pi n f)/[n \sin(\pi f)]$.

Fig. 3 provides an example of the estimated trend $\{\tilde{y}(i)\}$ (red dashed lines) when a sample path of Brownian motion (integration of white Gaussian noise) is analyzed by first-order DFA and by centered DMA. As shown in Fig. 3(a), the estimated trend $\{\tilde{y}(i)\}$ (red dashed lines) in DFA shows discontinuous jumps at the end points of each window. Moreover, as

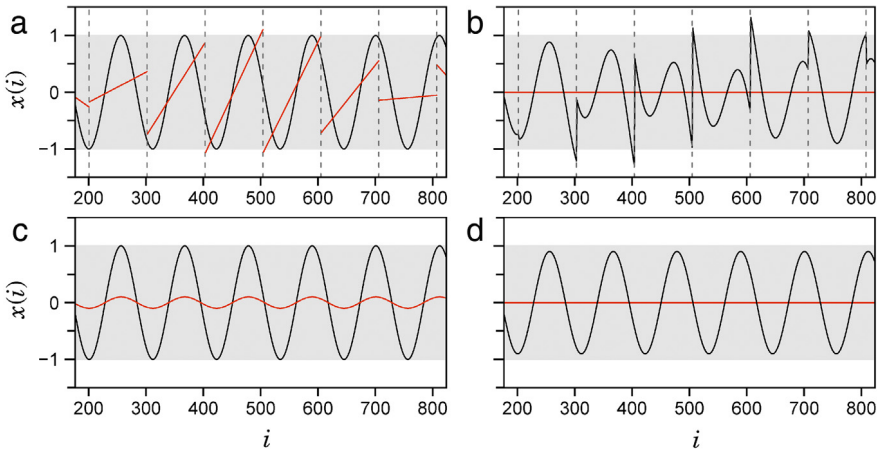

Fig. 1. Illustration of detrending filters in DFA (a, b) and DMA (c, d). A time series given by $x(i) = \sin(2\pi f t)$ with $f = 0.009$ [shown by black solid lines in (a) and (c)] is transformed by the detrending filter at scale $n = 101$. Red solid lines in (a) and (c) represent the estimated trend. Black solid lines in (b) and (d) represent the filtered output. (For interpretation of the references to color in this figure legend, the reader is referred to the web version of this article.)

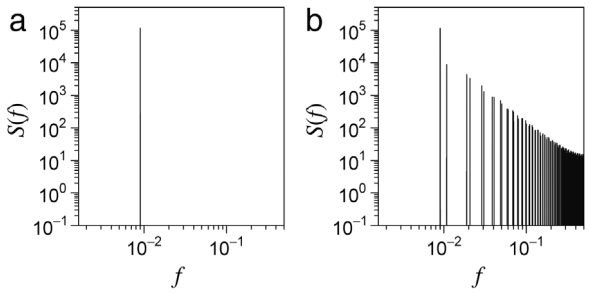

Fig. 2. Power spectral density functions $S(f)$ of a single-frequency time series with $f = 0.009$ (a) and its filtered output (b).

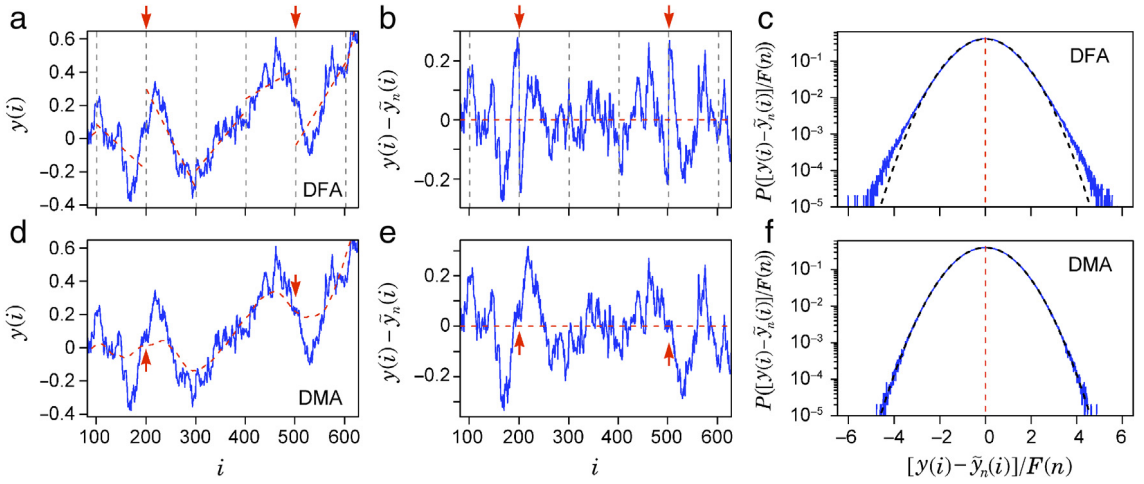

Fig. 3. Illustrative examples of deviations from the estimated trend. A sample path $\{y(i)\}$ of Brownian motion is analyzed at scale $n = 101$ by first-order DFA (top) and centered DMA (bottom). (a, d) A sample path $\{y(i)\}$ of Brownian motion (solid lines) and the estimated trend $\tilde{y}_n(i)$ (dashed lines). (b, e) Deviations from the estimated trend (solid lines). (c, f) Probability distributions of the deviations (solid lines). For comparison, we also show a Gaussian distribution (dashed lines). (For interpretation of the references to color in this figure legend, the reader is referred to the web version of this article.)

indicated by the arrows in Fig. 3(b), deviations from the estimated trend, $\{y(i) - \tilde{y}(i)\}$, near the end points of each window show large variability [cf. Fig. 3(e)]. As a result, the deviations, $\{y(i) - \tilde{y}(i)\}$, obey a non-Gaussian distribution [Fig. 3(c)] even when a Gaussian process is analyzed. The distribution of $\{y(i) - \tilde{y}(i)\}$ is deformed depending on the correlation property of $\{y(i)\}$. In contrast, the estimated trend $\{\tilde{y}(i)\}$ in centered DMA [Fig. 3(d)] shows seemingly continuous behavior. In addition,

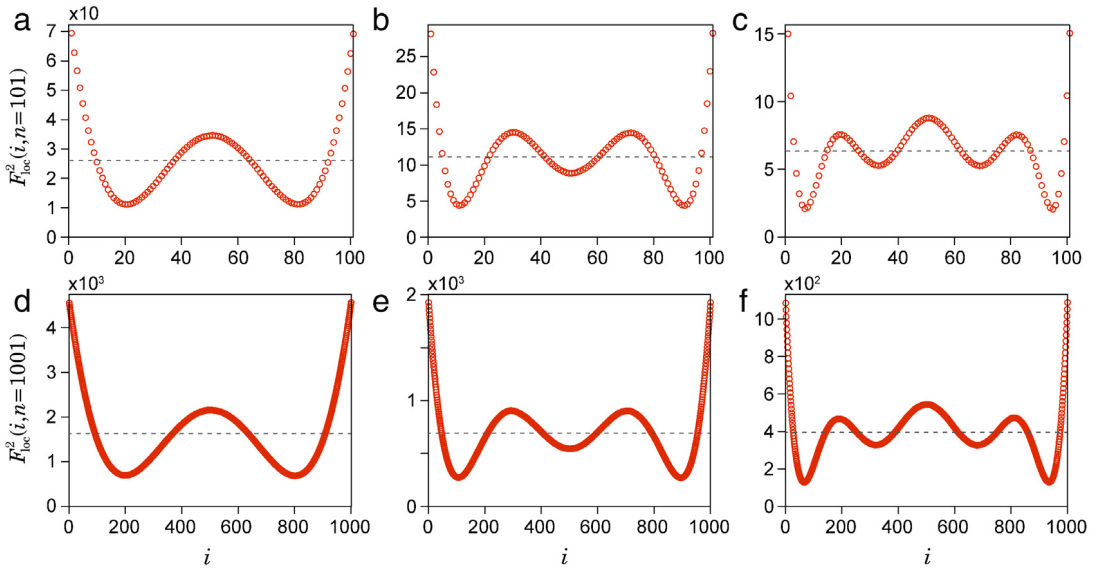

Fig. 4. Pointwise mean-square deviation $F^2_{\mathrm{loc}}(i;n)$ at (a–c) $n = 101$ and (d–f) $n = 1001$. $F^2_{\mathrm{loc}}(i;n)$ are numerically estimated by analyzing 10^5 samples of long-range correlated time series displaying $F(n) \sim n^{0.9}$ ($\alpha = 0.9$). (a, d) First-order DFA. (b, e) Second-order DFA. (c, f) Third-order DFA.

when a Gaussian process is analyzed by DMA, deviations from the estimated trend, $\{y(i) - \tilde{y}(i)\}$, obey a Gaussian distribution [Fig. 3(f)].

To understand in more detail the nonlinear filtering properties of DFA, we consider the pointwise mean-square deviation within a segment (window). The pointwise mean-square deviation is defined as

$$F^2_{\mathrm{loc}}(i;n) = \left\langle \left(y(i) - \tilde{y}(i)\right)^2 \right\rangle \quad \text{for } 1 \le i \le n, \tag{4}$$

where $\langle \cdot \rangle$ denotes an ensemble average and $\{\tilde{y}(i)\}$ is the least-squares polynomial fit to $y(i)$ in this segment. Fig. 4 shows illustrative examples of numerically estimated $F^2_{\mathrm{loc}}(i;n)$ when a long-range correlated time series displaying $F(n) \sim n^{0.9}$ is analyzed. As shown in Fig. 4, the local square deviations over a segment are nonuniformly distorted, depending on the order of DFA. Especially, the deviations near both end points are extremely enlarged.

To evaluate the statistical bias induced by the DFA detrending filter, we numerically estimate the maximum and minimum values of $F^2_{\mathrm{loc}}(i;n)/F^2(n)$, where $F^2(n)$ is calculated by

$$F^2(n) = \frac{1}{n}\sum_{i=1}^{n} F^2_{\mathrm{loc}}(i;n). \tag{5}$$

As shown in Fig. 4, the maximum value always appears at both end points of a segment, and the minimum value appears as the outermost local minima. Fig. 5(a) shows the dependence of the maximum and minimum values of $F^2_{\mathrm{loc}}(i;n)/F^2(n)$ on the scale n. As shown in Fig. 5(a), the maximum and minimum converge to constant values as n increases. In contrast, as shown in Fig. 5(b), (c), and (d), the difference between the maximum and minimum values monotonically increases as α increases. Therefore, the statistical bias of the local square deviations becomes large when a time series with a large α is analyzed.

Next we analytically evaluate $F^2_{\mathrm{loc}}(i;n)$ of first-order DFA using a continuous time approximation and the single-frequency response [21]. First, let us consider the single-frequency component $x(t) = A\cos(2\pi f t + \theta)$, where A, f, and θ are constant parameters. After integration it can be written as

$$y(t) = \frac{A}{2\pi f}\sin(2\pi f t + \theta), \tag{6}$$

where the integral constant has been neglected. In the interval $[0, n]$, the least-squares line is obtained by minimizing the following function:

$$I(a_0, a_1) = \int_0^n \left\{ \frac{A}{2\pi f}\sin(2\pi f t + \theta) - (a_0 + a_1 t) \right\}^2 \mathrm{d}t. \tag{7}$$

Namely, we solve the following equations:

$$\frac{\partial I(a_0, a_1)}{\partial a_0} = 0, \qquad \frac{\partial I(a_0, a_1)}{\partial a_1} = 0, \tag{8}$$

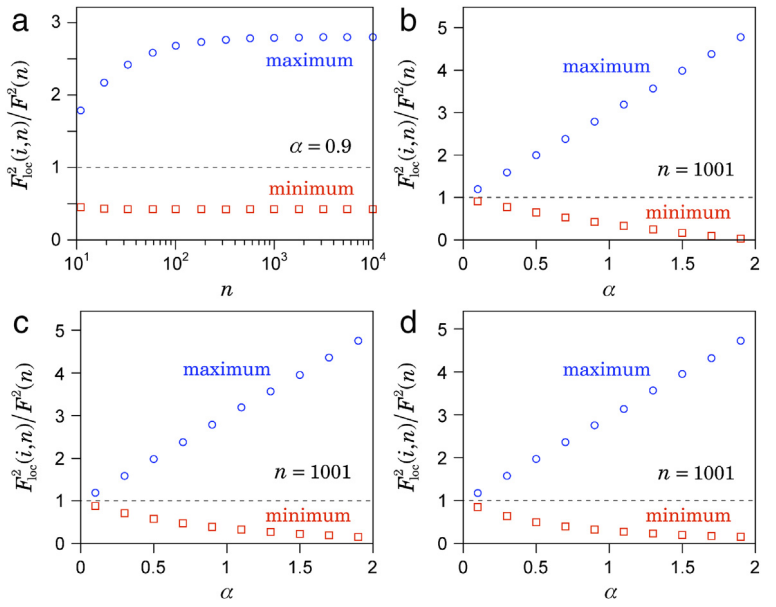

Fig. 5. The maximum and the minimum values of $F^2_{\rm loc}(i;n)/F(n)$. $F^2_{\rm loc}(i;n)$ and $F(n)$ are numerically estimated by analyzing 10^5 samples of long-range correlated time series displaying $F(n) \sim n^{\alpha}$. (a) The dependence on the scale n when a long-range correlated time series displaying $F(n) \sim n^{0.9}$ is analyzed. (b–d) The dependence on the scaling exponent α of the analyzed time series at the scale $n = 1001$. (b) First-order DFA. (c) Second-order DFA. (c) Third-order DFA.

and then obtain

$$a_0 = \frac{A\{2\pi fn\cos\theta + \pi fn\cos(2\pi fn+\theta) - 3\sin(\pi fn)\cos(\pi fn+\theta)\}}{2\pi^3 f^3 n^2}, \tag{9}$$

$$a_1 = -\frac{3A\cos(\pi fn+\theta)\{\pi fn\cos(\pi fn) - \sin(\pi fn)\}}{\pi^3 f^3 n^3}. \tag{10}$$

By using these results, the square deviation at $t \in [0, n]$ is given by

$$\Phi^2_{\rm loc}(t;n,f,A,\theta) = \left\{\frac{A}{2\pi f}\sin(2\pi ft+\theta) - (a_0 + a_1 t)\right\}^2. \tag{11}$$

Moreover, by averaging the phase θ over $[0, 2\pi]$, we could evaluate the local square deviation as

$$\begin{aligned}\overline{\Phi}^2_{\rm loc}(t;n,f,A) = \frac{A^2}{16\pi^6 f^6 n^6}\Big\{&36t^2\left(\pi^2f^2n^2+1\right) - 36nt\left(\pi^2f^2n^2+1\right)\\ &+\left(8\pi^2f^2n^4 - 36\pi^2f^2n^3t + 36nt - 36t^2\right)\cos(2\pi fn)\\ &+9n^2\left(4\pi^2f^2t^2-1\right)\cos(2\pi fn) + 4\pi^3f^3n^5\sin(2\pi f(n-t))\\ &-12\pi^3f^3n^4t\sin(2\pi f(n-t)) + 4\pi^3f^3n^4(3t-2n)\sin(2\pi ft)\\ &+6\pi^2f^2n^3(n-2t)\cos(2\pi f(n-t)) - 18\pi fn^3\sin(2\pi fn)\\ &-6\pi^2f^2n^3(n-2t)\cos(2\pi ft) - 72\pi ft^2\sin(2\pi fn)\\ &+72\pi fn^2t\sin(2\pi fn) + n^2\left(2\pi^4f^4n^4 + 10\pi^2f^2n^2+9\right)\Big\}.\end{aligned} \tag{12}$$

Based on Eq. (12) and the Fourier amplitude spectrum of a linear stochastic process, the pointwise mean-square deviation is estimated as

$$F^2_{\rm loc}(i;n) \approx \sum_{k=1}^{\lfloor N/2\rfloor} \overline{\Phi}^2_{\rm loc}(i;n,A_k,f_k), \tag{13}$$

where k is the number of the Fourier component and $\lfloor\cdot\rfloor$ is the floor function.

As an example, let us consider the analysis of a white Gaussian process with variance σ_0^2. In this case, the pointwise mean-square deviation is given by

$$F^2_{\rm loc}(i;n) \approx \sum_{k=1}^{(n-1)/2} \overline{\Phi}^2_{\rm loc}(i;n,A_0,k/n), \tag{14}$$

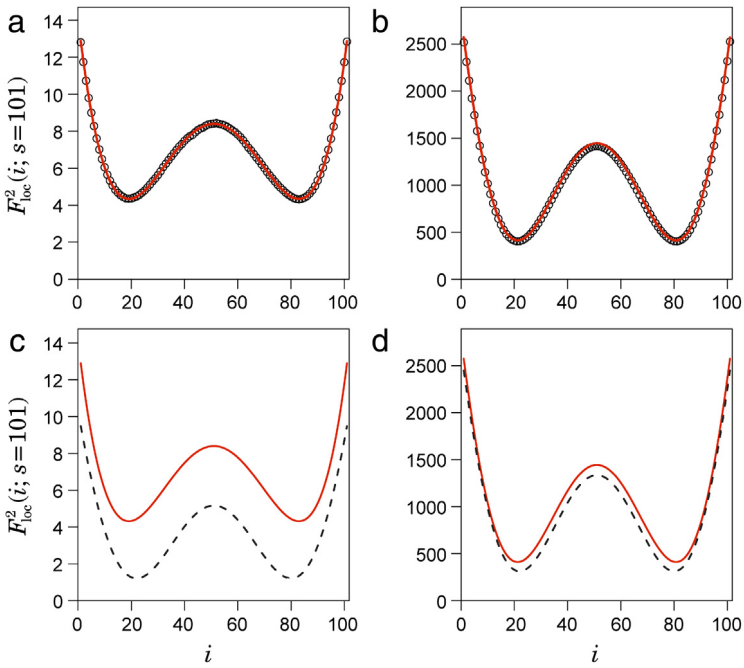

Fig. 6. Pointwise mean-square deviation $F^2_{\rm loc}(i; n = 101)$ in first-order DFA. $F^2_{\rm loc}(i; n)$ (solid lines) are analytically estimated by using Eqs. (12) and (13). Circles in (a) and (b) represent numerically estimated results based on Monte Carlo experiments. (a, c) A white Gaussian process ($\alpha = 0.5$) with $A_k(f_k) \sim$ constant. (b, d) A Brownian motion process ($\alpha = 1.5$) with $A_k(f_k) \sim f_k^{-1}$. Dashed lines in (c) and (d) represent the pointwise mean-square deviation of the lowest frequency component. (For interpretation of the references to color in this figure legend, the reader is referred to the web version of this article.)

where $A_0^2 = 4\sigma_0^2/(n-1)$ and n is assumed to be an odd integer. As shown in Fig. 6(a), the analytical prediction (red solid lines) by Eq. (14) is in excellent agreement with the numerical result (circles) based on Monte Carlo experiments. Results for a Brownian motion process are also shown in Fig. 6(b). It is important to note that the nonuniformly weighted local square deviations are mainly generated by low frequency components. Namely, as shown in Fig. 6(c) and (d), the shape of the pointwise mean-square deviation (red solid lines) is mainly dominated by square deviations of the lowest frequency component (dashed lines). Therefore, as the relative contribution of low-frequency components increases, the nonuniformity of $F^2_{\rm loc}(i; n)$ appears more dominantly. In contrast, in centered DMA, such nonuniformity does not exist.

4. Estimation instability induced by piecewise least-squares fitting

The nonuniformly weighted estimation of the root-mean-square deviation may induce accidental estimation errors. To investigate this, using first-order DFA and centered DMA, we analyze a numerically generated time series displaying intermittent fluctuations [24,25], as shown in Fig. 7. The time series is generated based on the idea of the multiplicative random cascade (see Ref. [24] for details) and is given by

$$x(i) = \xi(i) \exp\left[\sum_{j=1}^{m} \omega^{(j)} \left(\left\lfloor \frac{i-1}{2^{m-j}} \right\rfloor \right)\right], \tag{15}$$

where ξ and $\omega^{(j)}$ are both Gaussian random variables and m is the total number of cascade steps. In this process, the probability density function (PDF) of $\{x(i)\}$ displays a non-Gaussian shape with fat tails, depending on the shape parameter λ_0^2, indicating the variance of $\omega^{(j)}$. When $\lambda_0^2 = 0$ [Fig. 7(a)], the PDF obeys a Gaussian distribution. In contrast, a larger value of λ_0^2 means that the time series displays intermittent bursts [Fig. 7(b) and (c)] and that its PDF has fatter tails and a sharper peak in comparison with the Gaussian distribution. In our numerical study, $\{\xi(i)\}$ is assumed to be a white Gaussian random variable. Therefore, the analytical value of the scaling exponent α is equal to 0.5.

Fig. 8 shows plots of $\log_{10} F(n)$ vs. $\log_{10} n$ and local slopes of $\log_{10} F(n)$, where the local slope is calculated by using two adjacent points on $\log_{10} F(n)$. For first-order DFA, as shown in Fig. 8(d), (e), and (f), local slopes of $\log_{10} F(n)$ exhibit widely scattered behavior. Moreover, larger intermittent bursts in the analyzed time series [Fig. 7(b) and (c)] result in more widely scattered behavior of the local slopes [Fig. 8(e) and (f)]. In contrast, for centered DMA, local slopes of $\log_{10} F(n)$ exhibit smoother behavior. In addition, the effect of large intermittent bursts is not evident.

To provide a quantitative characterization of the estimation instability of first-order DFA and centered DMA, we numerically estimated the mean absolute difference between estimated local slopes of $\log_{10} F(n)$ and the analytically

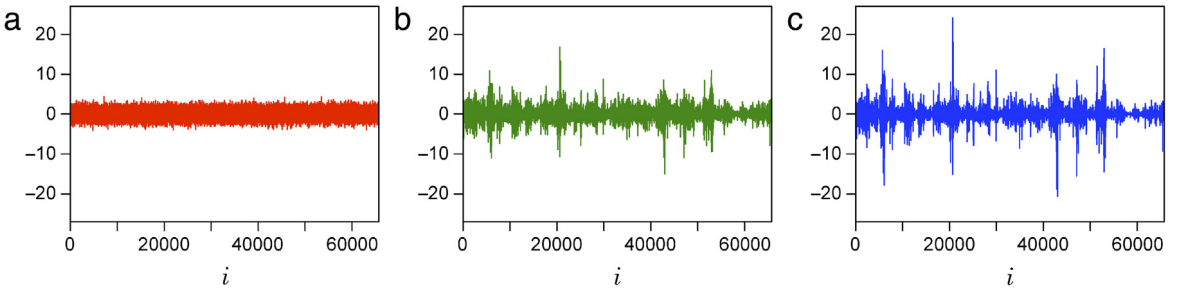

Fig. 7. Time series of the multiplicative cascade process. (a) $\lambda_0 = 0$ (white Gaussian process). (b) $\lambda_0 = 0.5/16$ and $m = 16$. (c) $\lambda_0 = 1.0/16$ and $m = 16$. The length of each time series is equal to $2^{16} = 65\,536$.

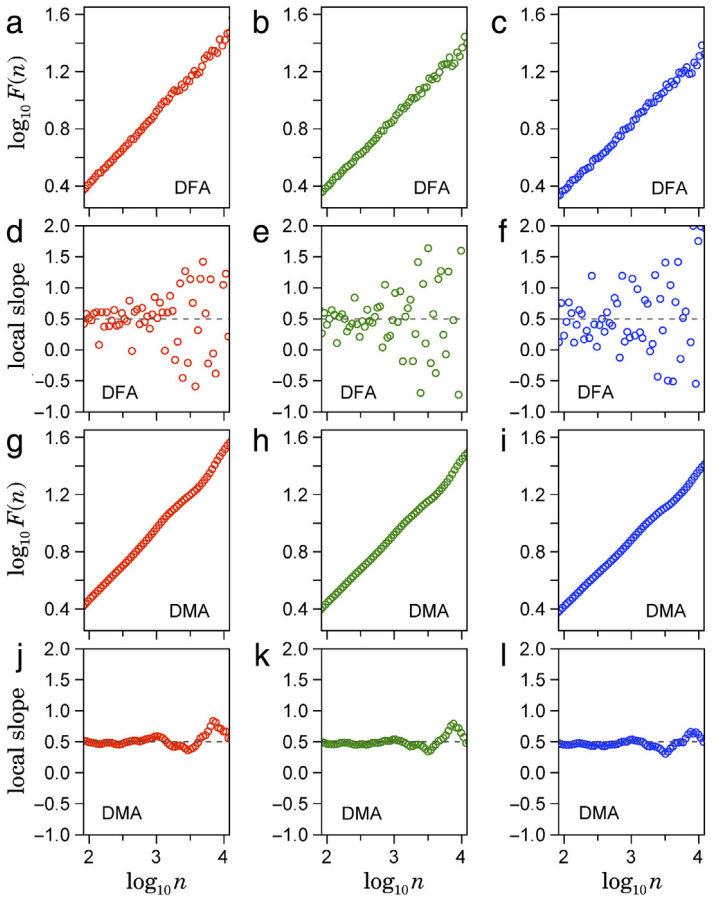

Fig. 8. Plots of $\log_{10} F(n)$ vs. $\log_{10} n$ and local slopes of $\log_{10} F(n)$, when the time series shown in Fig. 7 are analyzed by first-order DFA (a–f) and by centered DMA (g–l). The local slope is calculated by using two adjacent points on $\log_{10} F(n)$. (Left) Results for Fig. 7(a). (Middle) Results for Fig. 7(b). (Right) Results for Fig. 7(c).

predicted slope ($\alpha = 0.5$) using 1000 samples for each condition. In addition, a sliding window DFA using overlapping segments shifted point by point was also investigated. In the case of the sliding window DFA, 200 samples for each condition were analyzed. As shown in Fig. 9, the local slopes estimated by using a first-order DFA (Fig. 9(a)) exhibit a much larger variability than those estimated by using a centered DMA (Fig. 9(b)) and sliding window DFA (Fig. 9(c)). As a quantitative parameter to characterize the scattered behavior of $\log_{10} F(n)$, we further calculate the standard deviation of the increments of $\log_{10} F(n)$ over the range of $N/10^2 \leq n \leq N/10$, where N is the data length, and the analyzed scales are integers nearest to the geometric progression with a common ratio of $2^{1/8}$. This parameter is denoted by σ_Δ. As shown in Fig. 10(a), σ_Δ estimated by using a first-order DFA (circles) is approximately proportional to the non-Gaussian parameter λ and exhibits much larger values than those estimated by using a centered DMA (triangles) and sliding window DFA (squares). Furthermore, as shown in Fig. 10(b), σ_Δ estimated by using the DFA (circles) rapidly increases in proportion to α of the analyzed time series.

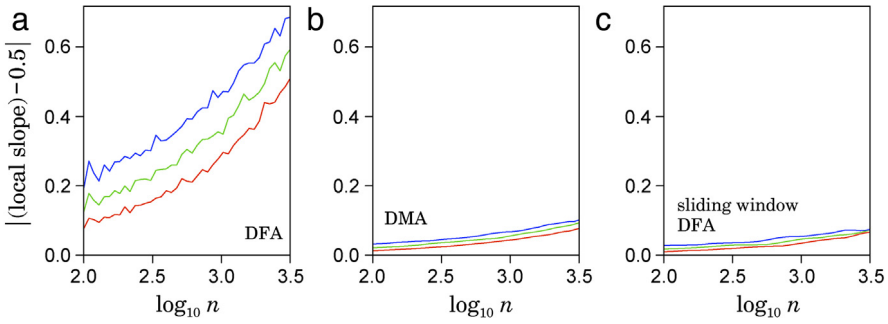

Fig. 9. Mean absolute difference between estimated local slopes of $\log_{10} F(n)$ and the analytically predicted slope ($\alpha = 0.5$). The colors represent conditions of the corresponding colors in Fig. 7. (a) First-order DFA. (b) Centered DMA. (c) Sliding window DFA. (For interpretation of the references to color in this figure legend, the reader is referred to the web version of this article.)

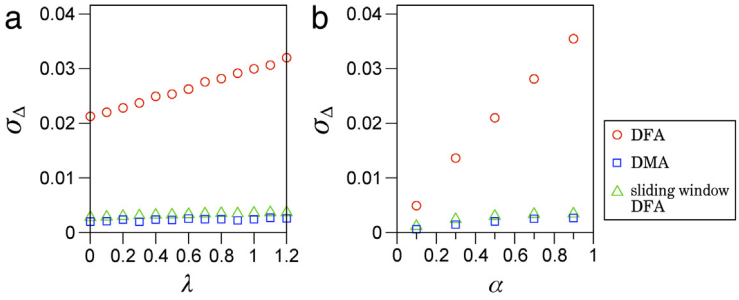

Fig. 10. Standard deviation of the increments of $\log F(n)$ over the range of $N/10^2 \leq n \leq N/10$, denoted by σ_Δ, where N is the data length. (a) The dependence of σ_Δ on the non-Gaussian parameter λ of multiplicative cascade processes with $\lambda_0 = \lambda/16$. (b) The dependence of σ_Δ on the scaling exponent α of a Gaussian process.

Our results demonstrate that, because of the nonlinear detrending filter in the DFA, large intermittent bursts and the strong long-range correlation in the time series result in an increase in the local slope variability. In contrast, in the centered DMA and sliding window DFA, the local slope variability is much smaller than that of the DFA. The estimation instability observed in DFA would be a disadvantage of the method and improvement is needed.

5. Summary and discussion

In this paper, we have investigated properties of the nonlinear detrending filter in DFA and found that it results in a nonuniformly weighted estimation of the root-mean-square deviation. Because of this property, large intermittent bursts and a strong long-range correlation in the analyzed time series could induce an increase in the slope estimation error. From a statistical viewpoint, this property is unfavorable. It has also been shown that, in comparison with the first-order DFA, the centered DMA and sliding window DFA have better statistical properties such as the uniformity of the square deviation estimation and less sensitivity to large intermittent bursts and the strong long-range correlation in the analyzed time series.

Our results have shown that a methodological improvement in the DFA, especially its detrending procedure, is still required. Although, as shown in this paper, a sliding window DFA could avoid the nonuniformly weighted estimation of the root-mean-square deviation, this approach would require a much larger computational cost. Recently, mth-order centered DMA, where m is a nonnegative even integer, has been shown to be very well comparable with that of $(m + 1)$th-order DFA [23]. In addition, a fast algorithm for higher order DFA, whose computational cost is comparable to the original DFA, has been developed [26]. Therefore, higher order centered DMA might be regarded as an improved method of higher order DFA. However, filtering properties of higher order centered DMA have not been fully elucidated. In addition, the performance of other DFA variants using a different type of linear filter has not been systematically investigated. Therefore, further studies are required to improve the detrending filter properties in DFA methodology, including multifractal DFA [27] and detrended cross-correlation analysis [28].

Acknowledgments

The authors would like to thank Professors Anna Carbone, Taishin Nomura, and Yasuyuki Suzuki for fruitful comments. This work was supported by JSPS KAKENHI Grant Numbers 15K01285 and 26461094.

References

[1] C.-K. Peng, S.V. Buldyrev, S. Havlin, M. Simons, H.E. Stanley, A.L. Goldberger, Mosaic organization of DNA nucleotides, Phys. Rev. E 49 (1994) 1685.
[2] C.-K. Peng, S. Havlin, H.E. Stanley, A.L. Goldberger, Quantification of scaling exponents and crossover phenomena in nonstationary heartbeat time series, Chaos 5 (1995) 82–87.
[3] J.W. Kantelhardt, E. Koscielny-Bunde, H.H. Rego, S. Havlin, A. Bunde, Detecting long-range correlations with detrended fluctuation analysis, Physica A 295 (2001) 441–454.
[4] G. Rangarajan, M. Ding, Integrated approach to the assessment of long range correlation in time series data, Phys. Rev. E 61 (2000) 4991–5001.
[5] H.E. Hurst, Long-term storage capacity of reservoirs, Trans. Amer. Soc. Civil Eng. 116 (1951) 770–808.
[6] E. Alessio, A. Carbone, G. Castelli, V. Frappietro, Second-order moving average and scaling of stochastic time series, Eur. Phys. J. B 27 (2002) 197–200.
[7] A. Carbone, G. Castelli, H. Stanley, Analysis of clusters formed by the moving average of a long-range correlated time series, Phys. Rev. E 69 (2004) 026105.
[8] K. Kiyono, Z.R.N.A. Struzik, F. Togo, Y. Yamamoto, Phase transition in healthy human heart rate, Phys. Rev. Lett. 95 (2005) 058101.
[9] C. Chianca, A. Ticona, T. Penna, Fourier-detrended fluctuation analysis, Physica A 357 (2005) 447–454.
[10] J. Alvarez-Ramirez, E. Rodriguez, J.C. Echeverría, Detrending fluctuation analysis based on moving average filtering, Physica A 354 (2005) 199–219.
[11] E. Rodriguez, J.C. Echeverria, J. Alvarez-Ramirez, Detrending fluctuation analysis based on high-pass filtering, Physica A 375 (2007) 699–708.
[12] X.-Y. Qian, G.-F. Gu, W.-X. Zhou, Modified detrended fluctuation analysis based on empirical mode decomposition for the characterization of anti-persistent processes, Physica A 390 (2011) 4388–4395.
[13] K. Hu, P.C. Ivanov, Z. Chen, P. Carpena, H.E. Stanley, Effect of trends on detrended fluctuation analysis, Phys. Rev. E 64 (2001) 011114.
[14] Z. Chen, P.C. Ivanov, K. Hu, H.E. Stanley, Effect of nonstationarities on detrended fluctuation analysis, Phys. Rev. E 65 (2002) 041107.
[15] Z. Chen, K. Hu, P. Carpena, P. Bernaola-Galvan, H.E. Stanley, P.C. Ivanov, Effect of nonlinear filters on detrended fluctuation analysis, Phys. Rev. E 71 (2005) 011104.
[16] L. Xu, P.C. Ivanov, K. Hu, Z. Chen, A. Carbone, H.E. Stanley, Quantifying signals with power-law correlations: A comparative study of detrended fluctuation analysis and detrended moving average techniques, Phys. Rev. E 71 (2005) 051101.
[17] A. Bashan, R. Bartsch, J.W. Kantelhardt, S. Havlin, Comparison of detrending methods for fluctuation analysis, Physica A 387 (2008) 5080–5090.
[18] W. Rea, L. Oxley, M. Reale, J. Brown, Estimators for long range dependence: an empirical study. ArXiv preprint arXiv:0901.0762.
[19] Y.-H. Shao, G.-F. Gu, Z.-Q. Jiang, W.-X. Zhou, D. Sornette, Comparing the performance of FA, DFA and DMA using different synthetic long-range correlated time series, Sci. Rep. 2 (2012) 835.
[20] M.S. Taqqu, V. Teverovsky, W. Willinger, Estimators for long-range dependence: an empirical study, Fractals 3 (1995) 785–798.
[21] K. Kiyono, Establishing a direct connection between detrended fluctuation analysis and Fourier analysis, Phys. Rev. E 92 (2015) 042925.
[22] M. Höll, H. Kantz, The relationship between the detrendend fluctuation analysis and the autocorrelation function of a signal, Eur. Phys. J. B 88 (2015) 1–7.
[23] A. Carbone, K. Kiyono, Detrending moving average algorithm: Frequency response and scaling performances, Phys. Rev. E 93 (2016) 063309.
[24] K. Kiyono, Z.R. Struzik, Y. Yamamoto, Estimator of a non-Gaussian parameter in multiplicative log-normal models, Phys. Rev. E 76 (2007) 041113.
[25] K. Kiyono, Log-amplitude statistics of intermittent and non-gaussian time series, Phys. Rev. E 79 (2009) 031129.
[26] Y. Tsujimoto, Y. Miki, S. Shimatani, K. Kiyono, Fast algorithm for scaling analysis with higher order detrending moving average method, Phys. Rev. E 93 (2016) 053304.
[27] J.W. Kantelhardt, S.A. Zschiegner, E. Koscielny-Bunde, S. Havlin, A. Bunde, H.E. Stanley, Multifractal detrended fluctuation analysis of nonstationary time series, Physica A 316 (2002) 87–114.
[28] B. Podobnik, H.E. Stanley, Detrended cross-correlation analysis: a new method for analyzing two nonstationary time series, Phys. Rev. Lett. 100 (2008) 084102.